The Density and Pseudo-Phase-Space Density Profiles of CDM halos

Aaron D. Ludlow[1,*], Julio F. Navarro[2], Michael Boylan-Kolchin[3,4], Volker Springel[5,6], Adrian Jenkins[7], Carlos S. Frenk[7], and Simon D. M. White[3],

[1] *Argelander-Institut für Astronomie, Auf dem Hügel 71, D-53121 Bonn, Germany*
[2] *Dept. of Physics and Astronomy, University of Victoria, Victoria, BC, V8P 5C2, Canada*
[3] *Max-Planck-Institut für Astrophysik, Karl-Schwarzschild-Straße 1, 85740 Garching bei München, Germany*
[4] *Center for Galaxy Evolution, 4129 Reines Hall, University of California, Irvine, CA 92697, USA*
[5] *Heidelberg Institute for Theoretical Studies, Schloss-Wolfsbrunnenweg 35, 69118 Heidelberg, Germany*
[6] *Zentrum für Astronomie der Universität Heidelberg, ARI, Mönchhofstr. 12-14, 69120 Heidelberg, Germany*
[7] *Institute for Computational Cosmology, Dept. of Physics, Univ. of Durham, South Road, Durham DH1 3LE, UK*

2 February 2011

ABSTRACT

Cosmological N-body simulations indicate that the spherically-averaged density profiles of cold dark matter halos are accurately described by Einasto profiles, where the logarithmic slope is a power-law of adjustable exponent, $\gamma \equiv d \ln \rho / d \ln r \propto r^\alpha$. The pseudo-phase-space density (PPSD) profiles of CDM halos also show remarkable regularity, and are well approximated by simple power laws, $Q(r) \equiv \rho/\sigma^3 \propto r^{-\chi}$. We show that this is expected from dynamical equilibrium considerations, since Jeans' equations predict that the pseudo-phase-space density profiles of Einasto halos should resemble power laws over a wide range of radii. For the values of α typical of CDM halos, the inner Q profiles of equilibrium halos deviate significantly from a power law only very close to the center, and simulations of extremely high-resolution would be needed to detect such deviations unambiguously. We use an ensemble of halos drawn from the Millennium-II simulation to study which of these two alternatives describe best the mass profile of CDM halos. Our analysis indicates that at the resolution of the best available simulations, both Einasto and power-law PPSD profiles (with adjustable exponents α and χ, respectively) provide equally acceptable fits to the simulations. A full account of the structure of CDM halos requires understanding how the shape parameters that characterize departures from self-similarity, like α or χ, are determined by evolutionary history, environment or initial conditions.

Key words: cosmology: dark matter – methods: numerical

1 INTRODUCTION

The large dynamic range probed by current simulations of structure formation allows for robust measurements of the internal structure of large samples of dark matter halos spanning a wide range of masses. The mass profile of CDM halos holds particular interest, mainly because of its direct connection with key observational probes of halo structure, such as disk galaxy rotation curves, gravitational lensing measurements, and more recently because of the possibility of observing the dark matter directly through its self-annihilation signal, or in laboratory detectors.

Navarro et al. (1996, 1997, hereafter, NFW) argued that the simple 2-parameter formula

$$\rho(r) = \frac{\rho_c}{r/r_s(1 + r/r_s)^2}, \qquad (1)$$

could be scaled to provide a good fit to the density profiles of simulated halos. The two physical scaling parameters are r_s, the radius where the logarithmic slope of the density profile, $\gamma \equiv d \log \rho / d \log r$, equals -2 (the isothermal value) and the characteristic density, ρ_c. As discussed by NFW, the parameters, r_s and ρ_c, are not independent but rather reflect the formation history of a given halo (see also, Kravtsov et al. 1997; Avila-Reese et al. 1999; Jing 2000; Bullock et al. 2001; Eke et al. 2001; Klypin et al. 2001).

* E-mail: aludlow@astro.uni-bonn.de

More recently, it has become clear that the mass profiles of CDM halos are *not* strictly self-similar, as originally suggested by NFW, but that a third parameter is actually required to describe their shape accurately (Navarro et al. 2004; Merritt et al. 2005, 2006; Gao et al. 2008; Hayashi & White 2008; Navarro et al. 2010). These studies have shown convincingly that profiles where the logarithmic slope is a simple power-law of radius, $\gamma = -2\,(r/r_{-2})^{\alpha}$, provide excellent fits to simulated halo profiles when the shape parameter α is allowed to vary. This implies a density profile of the form

$$\ln\left(\frac{\rho}{\rho_{-2}}\right) = -\frac{2}{\alpha}\left[\left(\frac{r}{r_{-2}}\right)^{\alpha} - 1\right], \tag{2}$$

which we call the "Einasto profile" for short (Einasto 1965). The Einasto and NFW parameters are simply related by $r_{-2} = r_s$ and $\rho_{-2} = \rho_c/4$.

A second result that has received widespread attention has been the fact that the pseudo-phase-space density (PPSD) profiles of simulated dark matter halos follow simple power-laws with radius:

$$Q(r) \equiv \frac{\rho}{\sigma^3} = \frac{\rho_0}{\sigma_0^3}\left(\frac{r}{r_0}\right)^{-\chi}. \tag{3}$$

This was originally reported by Taylor & Navarro (2001), and has been confirmed by a number of subsequent studies, albeit with some debate over the actual value of the best-fit power-law exponent (see, e.g., Rasia et al. 2004; Dehnen & McLaughlin 2005; Faltenbacher et al. 2007; Vass et al. 2009; Ludlow et al. 2010). Although originally shown to hold for the total velocity dispersion profile, eq. (3) also holds when σ is replaced with σ_r, the radial velocity dispersion (e.g., Dehnen & McLaughlin 2005; Navarro et al. 2010). (We hereafter use Q when referring to the total pseudo-phase-space density profile, and Q_r for its radial analog, ρ/σ_r^3.)

As discussed by Taylor & Navarro (2001), the power-law nature of Q does not fully determine the halo density profile. Indeed, a wide range of different density profiles are consistent with this constraint, even for spherically symmetric, isotropic systems in dynamical equilibrium. Well-behaved solutions, however, have only two possible asymptotic inner behaviours, one where the central density diverges like $\rho \propto r^{2\chi-6}$ (the singular isothermal sphere is an example, for $\chi = 2$), and another "critical" solution where the cusp asymptotic slope is much shallower; $\gamma \rightarrow -2\chi/5$ as $r \rightarrow 0$. Taylor & Navarro (2001) showed that the "critical" solution for $\chi = 1.875$ (the value predicted by the self-similar secondary infall solution studied by Bertschinger 1985) closely resembles the NFW profile over the radial range resolved by their simulations.

The inner asymptotic behaviour predicted by eqs. (2) and (3) for the density profile is therefore different (Einasto profiles have a finite-density core rather than a cusp), implying that simulations should be able to discriminate between the two. Indeed, the $Q(r)$ profiles of Einasto halos are *not* in general power-laws (Ma et al. 2009), which implies that halos cannot satisfy both eqs. (2) and (3) at once and that departures from either Einasto fits or power-law Q profiles should become apparent in simulations of adequate resolution.

Deviations from power laws in the *outer Q* profiles of simulated halos have already been reported by Ludlow et al. (2010), who argue that such departures are actually expected in regions near the virial boundary separating the inner equilibrium region from the unrelaxed infalling envelope of the halo. Whether similar deviations are also present in the inner regions of halos has not yet been studied in detail.

We address these issues here using a sample of equilibrium CDM halos selected from the Millennium-II (MS-II) simulation (Boylan-Kolchin et al. 2009). We begin in Section 2 with a brief description of our simulations and analysis techniques. Our main results are presented in Section 3; density profiles are presented in Section 3.1 and Q_r profiles in Section 3.2. Since both Einasto and power-law PPSD profiles are incomplete dynamical models unless the velocity anisotropy profile is specified we analyze this in Section 3.3. In Section 3.4 and 3.5 we compare the Einasto and power-law PPSD models and directly asses their ability to accurately describe the mass profiles of simulated halos. We end with a brief summary of our main conclusions in Section 4.

2   NUMERICAL SIMULATIONS

2.1   Cosmological model

Our analysis uses group and cluster halos identified in the MS-II, a $\sim 10^{10}$-particle cosmological simulation of the evolution of dark matter in a $100\ h^{-1}$ Mpc box. The run adopted a standard ΛCDM cosmogony with the same parameters as the Millennium simulation presented by Springel et al. (2005): $\Omega_{\rm M} = 0.25$, $\Omega_{\Lambda} = 1 - \Omega_{\rm M} = 0.75$, $n_s = 1$, $\sigma_8 = 0.9$, and a Hubble constant $H_0 \equiv H(z = 0) = 100\,h$ km s^{-1} Mpc^{-1} = 73 km s^{-1} Mpc^{-1}, but has better mass and spatial resolution. Interested readers may find further details in Boylan-Kolchin et al. (2009).

2.2   Halo selection

We base our results on a sample of well-resolved equilibrium halos in MS-II. We focus on halos where N_{200}, the number of particles within the virial radius[1], exceeds 5×10^5. This corresponds to group and cluster halos with virial masses above $\sim 3.44 \times 10^{12} h^{-1} {\rm M}_{\odot}$.

In addition we require our halos to satisfy the set of relaxation criteria introduced by Neto et al. (2007) in order to minimize the impact of transient departures from equilibrium on halo profiles. These criteria include limits on (i) the fraction of a halo's virial mass in self-bound substructures, $f_{\rm sub} = M_{\rm sub}(r < r_{200})/M_{200} < 0.07$; ii) the offset between a halo's center of mass and its true center (defined by the particle with the minimum potential energy), $d_{\rm off} = |\boldsymbol{r}_{\rm CM} - \boldsymbol{r}_{\rm cen}|/r_{200} < 0.05$, and iii) the virial ratio of kinetic to potential energies, $2K/|\Phi| < 1.3$. All dynamical quantities have been computed in the halo rest frame.

---

[1] The virial radius, r_{200}, defines the mass of a halo, M_{200}, as that of a sphere, centered at the potential minimum, whose enclosed density is 200 times the critical density for closure, $\rho_{\rm crit} = 3H^2/8\pi G$. $V_{200} = (GM_{200}/r_{200})^{1/2}$ is the halo's virial velocity.

With these selection criteria our sample consists of 440 halos, more than half of the total number of halos (790) in the same mass range.

2.3 Analysis

Our analysis deals with the spherically-averaged density, ρ, and velocity dispersion, σ, profiles of each of our 440 dark matter halos. Each profile is built out of 25 spherical shells equally spaced in $\log_{10} r$ spanning the range $r_{\rm conv} \leqslant r \leqslant r_{200}$. Here $r_{\rm conv}$ is the "convergence radius" defined by Power et al. (2003), where circular velocities converge to better than $\sim 10\%$. Each spherical shell is centered at the particle with the minimum potential energy, which we identify with the halo center.

For each radial bin we estimate the dark matter mass-density by dividing the total mass of the shell by its volume; the velocity dispersion is defined such that σ^2 is two times the specific kinetic energy in the shell, measured in the halo rest frame. Analogously, we compute the radial velocity dispersion, σ_r^2, in terms of the kinetic energy in radial motions within each shell. The velocity anisotropy parameter is defined by $\beta = 1 - \sigma_{\rm tan}^2/2\sigma_r^2$, where $\sigma_{\rm tan}^2 = \sigma^2 - \sigma_r^2$. The ρ and σ_r values in each radial shell are also used to estimate the pseudo-phase-space density profile, $Q_r(r) \equiv \rho/\sigma_r^3$. We choose to focus our analysis on the *radial* Q_r profiles (rather than the total $Q \equiv \rho/\sigma^3$) as this simplifies the analysis of Jeans' equations, in which the σ_r and $\beta(r)$ terms separate.

3 RESULTS

3.1 Density profiles

Figure 1 shows the spherically-averaged density profiles for halos in our sample, with the residuals from best-fit Einasto profiles shown in the middle panels. All profiles have been plotted from r_{200} down to the innermost resolved radius, $r_{\rm conv}$. Densities have been multiplied by r^2 in order to enhance the dynamic range of the graph and to highlight halo-to-halo differences. Einasto fits are limited to the radial range $r_{\rm conv} < r < 3\,r_{-2}$, so that their parameters are not unduly influenced by regions where crossing times are long, and dynamical equilibrium may not hold (Ludlow et al. 2010). Radii have been scaled to r_{-2}, the radius at which the logarithmic slope is equal to the isothermal value, -2, and densities by $\rho_{-2} \equiv \rho(r_{-2})$.

We assess the quality of fits to the density profiles using the following figure-of-merit function,

$$\psi^2 = \frac{1}{N_{\rm bin}} \sum_{i=1}^{N_{\rm bin}} (\ln \rho_i - \ln \rho_i^{\rm model})^2. \qquad (4)$$

All halos shown in Fig. 1 have $\psi_{\rm min} < 0.1$.

In order to highlight the differences in profile shape we have split our halo sample into three subsamples, each containing an equal number of halos: halos with $\alpha \leqslant 0.161$ are shown in red; green curves show those with $0.161 < \alpha \leqslant 0.195$, and blue curves are used for the rest. We adopt the same colour coding and halo samples in subsequent plots. For illustration, we also show three Einasto profiles with different values of the shape parameter, corresponding to the mean value of each halo subsample: $\alpha = 0.132$ (dashed curve), $\alpha = 0.178$ (solid black curve), and $\alpha = 0.230$ (dot-dashed curve).

The small residuals from best Einasto fits (typically less than 10% throughout the fitted region; see middle panels of Fig. 1) confirm that eq. (2) provides an excellent description of the density profiles of CDM halos down to the innermost resolved radius. Further, Figure 1 also demonstrates that there is genuine variation in profile shape from halo to halo: profiles of different halos "curve" differently, yielding best-fit α parameter values that range between roughly 0.1 and 0.25. The mass profiles of CDM halos are therefore *not* strictly self-similar, and α is a structural "shape" parameter genuinely needed to describe accurately the mass profile of CDM halos (see Navarro et al. 2010, for a full discussion).

### 3.2 Pseudo-phase-space density profiles

Fig. 2 shows the (radial) pseudo-phase-space density profiles, Q_r, of the halos in our sample, grouped as in Fig. 1. In order to take out the halo mass dependence, Q_r profiles have been scaled radially by r_{-2}, and vertically by ρ_{-2}/ν_{-2}^3, where $\nu_{-2} = \sqrt{G\,\rho_{-2}\,r_{-2}^2}$ is the characteristic velocity implied by the scale parameters ρ_{-2} and r_{-2}. Our results confirm the striking power-law nature of Q_r profiles previously reported in the literature. For reference, we also show the power law, $Q_r \propto r^{-1.875}$ (shown by a black dotted line), predicted by the self-similar solution of Bertschinger (1985).

In order to emphasize the differences between halos, we show in the middle panels of Fig. 2 the residuals from the Bertschinger power law normalized to the mean value of ρ_{-2}/ν_{-2}^3 for all halos in each sample. Although the residuals are in general small, the "curving" shape of their radial dependence provides a strong indication that the Q_r profiles of simulated CDM halos deviate systematically from a simple power-law of fixed exponent χ.

As discussed by Ludlow et al. (2010), the *outer* ($r \gg r_{-2}$) upturn in the residuals is most likely associated with the transition from the inner, relaxed parts, to the unrelaxed outer parts, where infalling material has not yet had time to phase-mix with the main body of the halo. Such an upturn is present also in the self-similar solution of Bertschinger (1985), and may be a general feature of the outer Q_r profiles of CDM halos. Because of this, we have chosen the radial range $r_{\rm conv} < r < 3\,r_{-2}$ for all the fits we report here.

Interestingly, the *inner* Q_r profiles ($r \lesssim 0.1\,r_{-2}$) also deviate from the $r^{-1.875}$ power law in a way that clearly depends on α. Note, for example, that at the innermost point the residuals of the lowest-α halos (leftmost middle panel in Fig. 2) are substantially larger than those of the largest-α halos (rightmost middle panel). We have explicitly verified that this α-dependence is *not* caused by grouping halos of different mass, nor by differences in numerical resolution. It is also unlikely to be due to anisotropies in the velocity distribution, since, as we show below, all halos in our sample are nearly isotropic at radii this close to the center. We have also checked that this α dependence is not specific to our choice of Q_r; the total pseudo-phase-space density profiles, $Q = \rho/\sigma^3$, follow similar trends with α.

These results imply that no single power-law can reproduce the radial dependence of the pseudo-phase-space density; if Q_r does indeed follow a power-law of radius, then
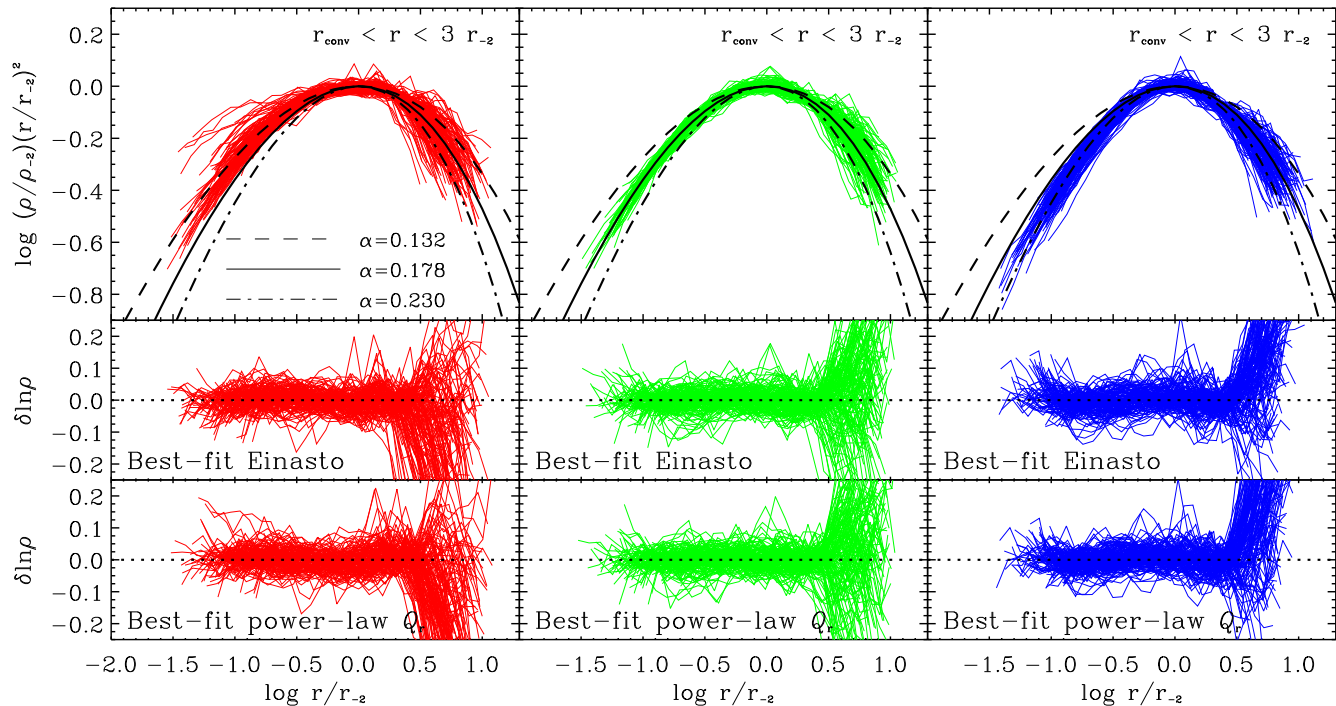
Figure 1. Spherically-averaged density profiles of all halos in our sample. All profiles are plotted over the radial range $r_{\rm conv} < r < r_{200}$. Radii have been scaled by r_{-2}; densities by $\rho_{-2} \equiv \rho(r_{-2})$. Density estimates have been multiplied by r^2 in order to increase the dynamic range of the plot so as to highlight differences between halos. The full sample of halos has been divided into three subsamples according to the best-fit value of the Einasto parameter α: red curves (left panels) correspond to halos with $\alpha \leqslant 0.161$; green curves (middle panels) to halos with $0.161 < \alpha \leqslant 0.195$ and blue curves (right panels) to halos with $\alpha > 0.195$. There are equal numbers of halos in each subsample. To illustrate the role of the shape parameter, α, Einasto profiles with $\alpha = 0.132$ (dashed), 0.178 (solid) and 0.230 (dot-dashed) are shown in the top panels. The middle panels are residuals from the best-fit Einasto profile with adjustable α; bottom panels are the residuals from the best-fit power-law Q_r "critical" model (see Sec. 3.4). In all cases fits are carried out over the radial range $r_{\rm conv} < r < 3\,r_{-2}$.

the exponent χ must vary from halo to halo. We show this explicitly in the bottom panels of Figure 2, where we plot the residuals from the best-fit power-law when the exponent χ is allowed to vary. The small residuals over the fitted radial range $r_{\rm conv} < r < 3\,r_{-2}$) indicate that a power-law with adjustable χ provides a remarkably accurate description of the inner Q_r profiles of CDM halos.

   Do Einasto profiles provide a better description of the spherically averaged structure of CDM halos than power-law Q_r profiles, or vice versa? Because of different dimensionality, we cannot compare directly the goodness of fits to the ρ and Q_r profiles shown in Figs. 1 and 2. One way to make progress is to compute the PPSD profiles corresponding to Einasto halos, or, alternatively, to compute the density profiles of power-law PPSD models and compare them with the simulations. This may be accomplished by assuming dynamical equilibrium and solving Jeans' equations to link the ρ and Q_r profiles, a procedure that, however, requires an assumption regarding the radial dependence of the velocity anisotropy, $\beta(r)$. We turn our attention to that issue next.

3.3   Velocity anisotropy

Velocity anisotropy profiles for all halos in our sample are shown in Figure 3, after rescaling all radii to r_{-2}. Halos have been grouped according to the value of the best-fit α

parameter, as in Figure 1. Solid lines with error bars show the median $\beta(r)$ profile of each group and the associated one-sigma scatter. The velocity anisotropy profiles exhibit a characteristic shape: they are isotropic near the center, become increasingly radial with increasing distance, before leveling off or becoming less anisotropic in the outskirts.

   Figure 4 shows the logarithmic slope-velocity anisotropy (γ vs β) relation for the median profiles of each halo subsample using the same colour coding as previous plots. The dotted line shows the linear $\beta(\gamma)$ relation proposed by Hansen & Moore (2006), which reproduces our simulation data well within the halo scale radius r_{-2} (i.e., for $\gamma > -2$).

   The data in Fig. 4 also suggests that the $\beta(\gamma)$ relation deviates from the Hansen & Moore fit in the outer regions (where β tends to a constant rather than the steadily increasing radial anisotropy predicted by Hansen & Moore). This dependence is captured well by the function

$$\beta(\gamma) = \frac{\beta_\infty}{2}\left(1 + \mathrm{erf}(\ln[(A\gamma)^2])\right), \qquad (5)$$

as shown by the dot-dashed curves in Figure 4. The values of β_∞ and A depend weakly but systematically on α, and are listed in Table 1. The radial β profiles corresponding to eq. (5) are also shown with dot-dashed curves in each panel of Figure 3, assuming that $\gamma(r)$ is given by the average Einasto profile of each grouping.
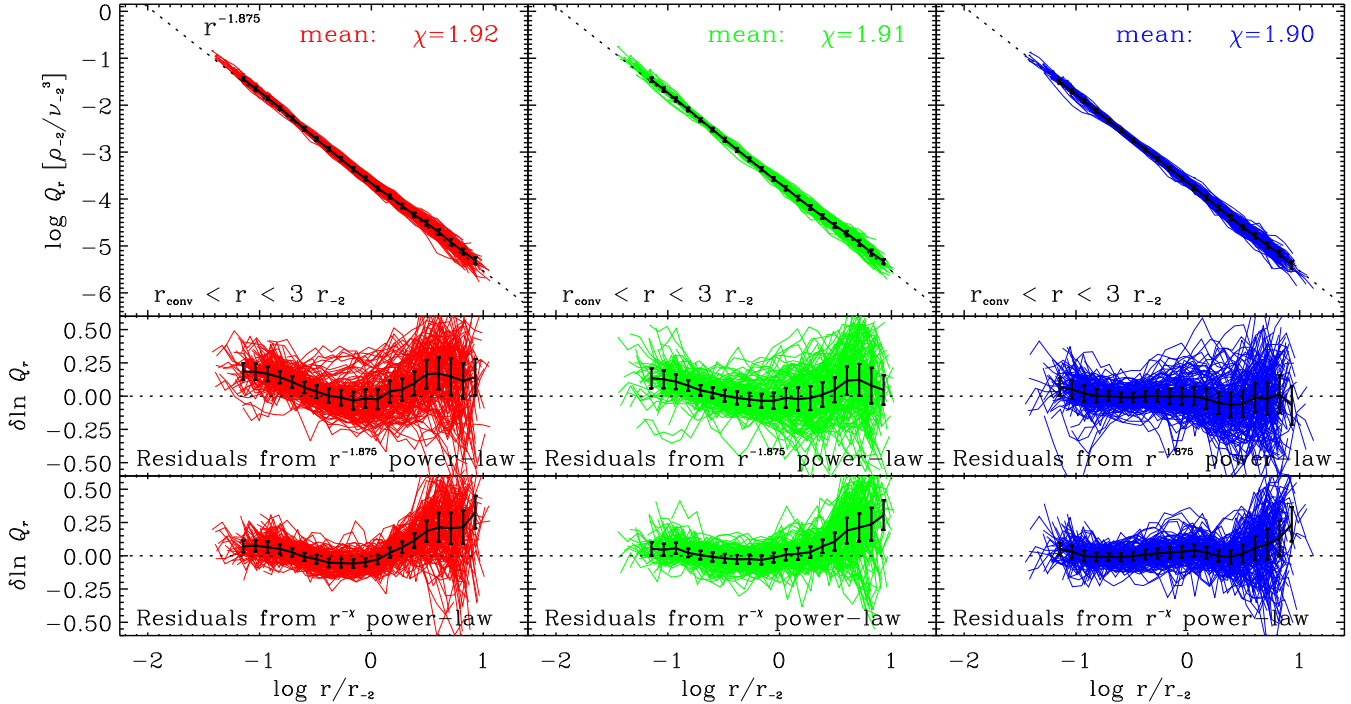
Figure 2. Radial pseudo-phase-space density profiles, $Q_r = \rho/\sigma_r^3$, for all halos in our sample. As in Fig. 1, halos are subdivided into three separate subsamples according to the value of their best-fit Einasto parameter α. Radii have been scaled by r_{-2}, densities by ρ_{-2} and velocities by $\nu_{-2} = \sqrt{G\rho_{-2}\, r_{-2}^2}$. The mean profiles and one-sigma scatter are shown as solid lines with error bars. The dotted curves in the top panels show a Bertschinger $r^{-1.875}$ power-law to guide the eye. The middle panels plot the residuals from the Bertschinger law normalized to the mean value of ρ_{-2}/ν_{-2}^3 for all halos in each sample. Lower panels show the residuals from the best-fit power-law, $r^{-\chi}$, with free-floating exponent, χ. Fits are limited to the radial range $r_{\rm conv} < r < 3\,r_{-2}$. The α-dependence of the Q_r profiles is clearly evident from the systematic differences in the shape of the residual curves shown in the middle panels.
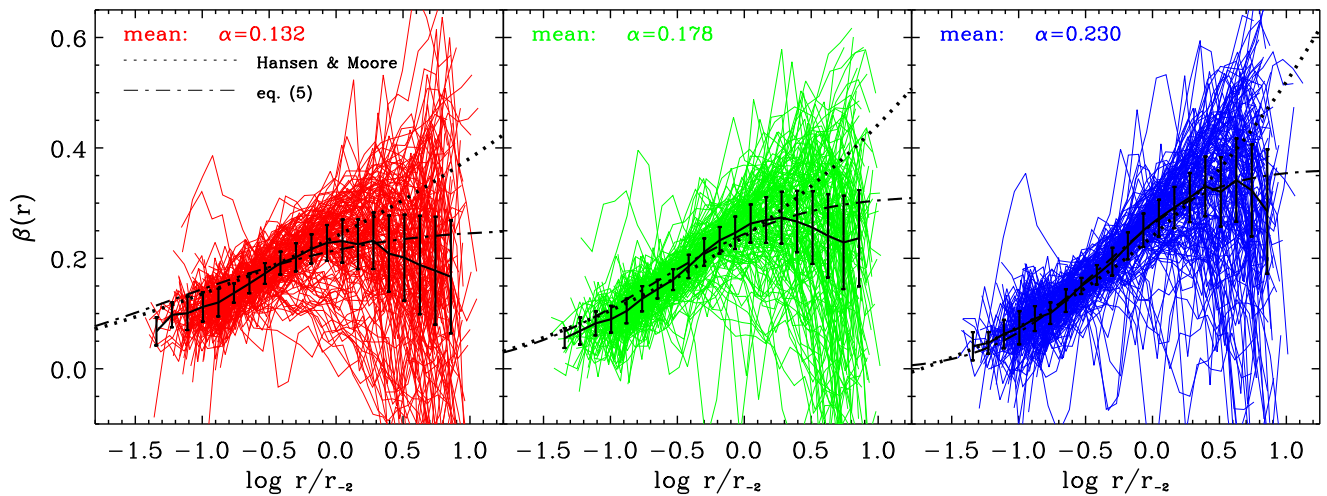
Figure 3. Velocity anisotropy profiles, $\beta = 1 - \sigma_{\rm tan}^2/2\sigma_r^2$, for all halos in our sample. Profiles have been grouped according to the best-fit Einasto parameter, as in Figure 1. Solid black lines with error bars show the median anisotropy profile and one-sigma dispersion for each halo subsample. The dot-dashed curves shown in each panel show the radial dependence of $\beta(r)$ expected from eq. (5) assuming the average Einasto density profile; dotted curves show $\beta(r)$ expected from Hansen & Moore (2006) for the same $\rho(r)$.
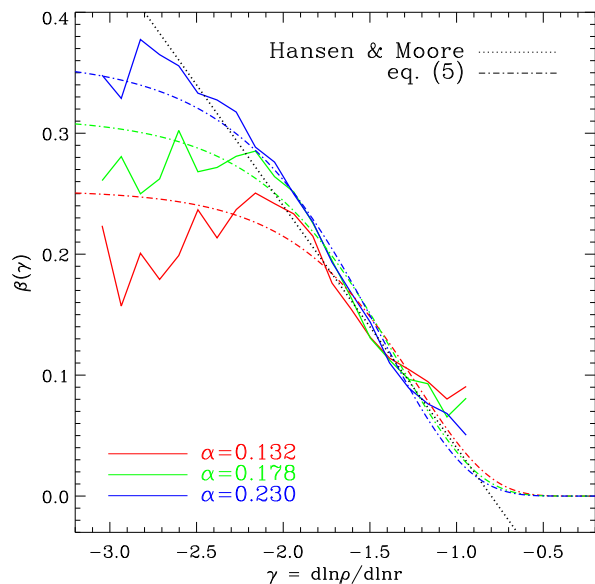
Figure 4. Median density slope-velocity anisotropy relation for the three groups of halos shown in previous figures. The linear $\beta - \gamma$ relation proposed by Hansen & Moore (2006) is shown as a dotted line; a relation of the form given in eq. (5) is shown separately for each sample using dot-dashed curves. There is some evidence that the mean $\beta - \gamma$ relation departs from the Hansen & Moore (2006) result in the outer regions of our halos. See text for further discussion.

3.4 Density profiles from power-law PPSD profiles

Once the radial dependence of the velocity anisotropy has been specified, equilibrium density profiles consistent with a power-law $Q_r(r)$ profile may be obtained from Jeans' equation. Following Dehnen & McLaughlin (2005), we write Jeans' equation as

$$\left(\gamma' - \frac{6}{5}\beta'\right) \quad + \quad \frac{2}{3}\left(\gamma + \chi + \frac{3}{2}\right)\left(\gamma + \frac{2}{5}\chi + \frac{6}{5}\beta\right)$$
$$= \quad -\frac{3}{5}\kappa_{-2}\, x^{2-2\chi/3} y^{1/3}, \tag{6}$$

where $y \equiv \rho/\rho_{-2}$; $x \equiv r/r_{-2}$; $\kappa_{-2} \equiv 4\pi G\rho_{-2}r_{-2}^2/\sigma_{r,-2}^2$ is a measure of the velocity dispersion in units of the "natural" velocity scale of the halo at r_{-2}, and we have assumed that $Q_r(r)$ is a power law of exponent χ. The logarithmic slope, $d\ln\rho/d\ln r$ is denoted by γ, and primes indicate derivatives with respect to $\ln x$. Once $\beta(r)$ is specified, the solution set of eq. (6) for given χ is fully characterized by κ_{-2}.

It is instructive to consider the special case $\beta(r) = 0$, for which three central asymptotic behaviours are possible: (i) a steep central cusp, $\gamma \to 2\chi - 6$; (ii) a central "hole" where $y(0) = 0$; or (iii) a "critical" solution with a shallow central cusp, $\gamma \to -2\chi/5$. The latter may be thought of as the limiting case where the radius of the central "hole" solution goes to zero, and corresponds to a maximally-mixed state for given halo binding energy and mass (Taylor & Navarro 2001).

Given that steep central cusps such as those in (i) are firmly ruled out by the data (see, e.g., Navarro et al. 2010), the "critical" solutions (iii) are the only viable density

profiles consistent with the power-law PPSDs constraint. Although these considerations are strictly true only for isotropic systems, similar conclusions apply once $\beta(r)$ is specified. This is especially true considering that halos are very nearly isotropic close to the center (see Sec. 3.3). We shall hereafter adopt the "critical" solutions (evaluated numerically) as the density profiles corresponding to a power-law PPSD profile for a given value of χ.

The left panel of Figure 5 shows (in blue) the "critical" density profiles for three different values of χ, and compares them to Einasto profiles. The values of α of the three Einasto profiles shown have been chosen to match as closely as possible the profiles corresponding to the PPSD models.

Clearly, for every value of χ it is possible to choose a value of α that matches the resulting density structure over a very wide range in radius. Deviations are only seen in the very inner regions, at less than 0.1% of the scale radius and therefore well outside the convergence region of any published halo simulation to date. For example, the black solid line in Fig. 5 shows the density profile of the billion-particle Aq-A-1 halo, whose convergence radius is roughly $0.01\,r_{-2}$ (Navarro et al. 2010). An Einasto profile with $\alpha = 0.17$ and a "critical" solution for $\chi = 1.911$ match the profile of this halo indistinguishably well.

3.5 PPSD profiles from Einasto profiles

Pseudo-phase-space density profiles corresponding to Einasto models can also be obtained by solving Jeans' equation, which may be written as follows:

$$\frac{d\ln\zeta_r^2}{d\ln r} - \zeta_r^2 = \gamma + \frac{d\ln V_c^2}{d\ln r} + 2\beta, \tag{7}$$

where $\zeta_r^2 \equiv V_c^2/\sigma_r^2$. With $\beta(r)$ set by eq. (5), the right hand side of this equation is fully specified by r_{-2}, ρ_{-2}, and α. Solutions may therefore be found after choosing the value of ζ_r (or its logarithmic derivative) at some fiducial radius, such as $\zeta_{-2} = \zeta_r(r_{-2})$. The shape of the Q_r profile is dictated by ζ_{-2}, and it is not generally a power law (Ma et al. 2009).

Again, insight may be gained by considering the limiting behaviour of the isotropic solutions. Because Einasto profiles have finite central densities, σ_r must approach a constant at the center. The central velocity dispersion may be found numerically, and turns out to be quite insensitive to ζ_{-2} (for given ρ_{-2}, r_{-2}, and α), provided that the ζ_{-2} is greater than about a tenth. (All of our halos are comfortably in that regime; indeed, the median value of ζ_{-2} for all of our halos is 1.274.) The finite value of the central velocity dispersion and its near invariance with ζ_{-2} also imply that the shape of the inner velocity dispersion profile is quite insensitive to the actual value of ζ_{-2}.

Therefore there is, in practice, a unique Q_r profile that corresponds to an Einasto profile of given α, which we identify with the single solution that is well behaved at all radii. This may be found by setting $d\ln\zeta_r^2/d\ln r = \alpha$ at $r = \infty$; for $\alpha = 0.175$, for example, this implies $\zeta_{-2} = 1.265$.

The right panel of Figure 5 shows (in red) the PPSD profiles of Einasto halos, for three different values of α. For $\alpha = 0.1$ and 0.17 the corresponding PPSD profiles are very well approximated by power laws over the whole plotted radial range. Only for larger values of α, such as 0.3, are clear deviations from a power law noticeable. Even in this case,
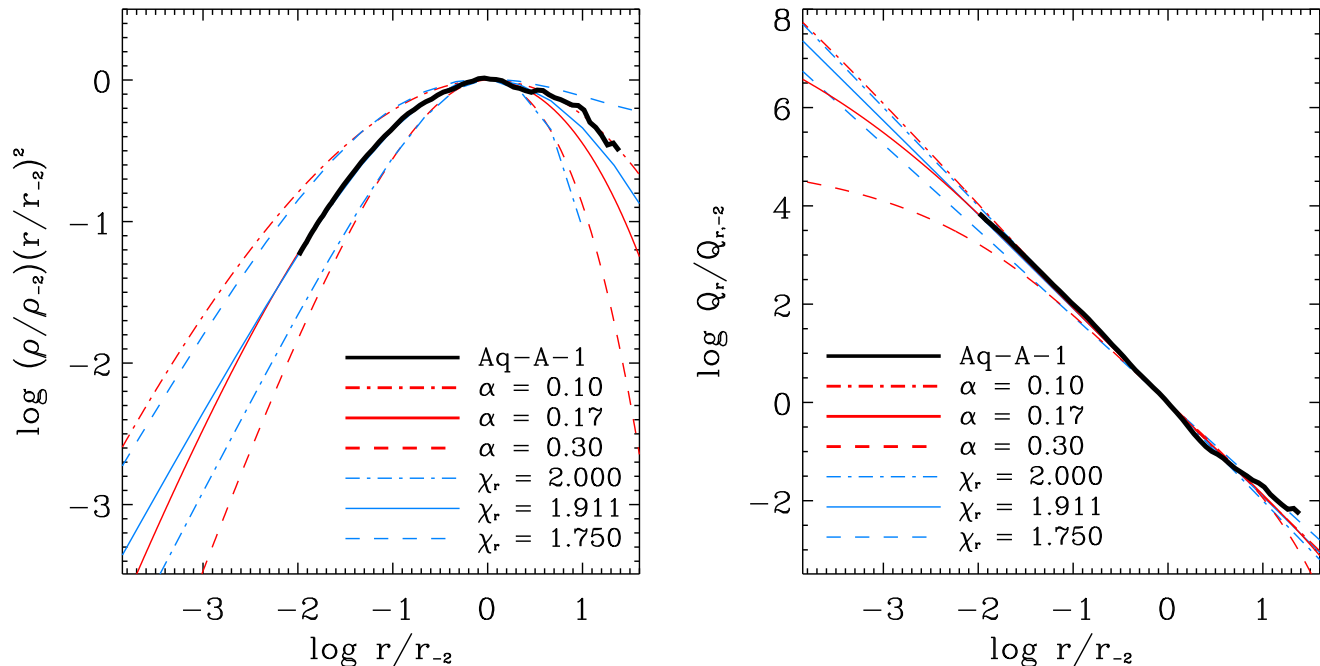
Figure 5. *Left:* Einasto density profiles compared with "critical" profiles computed from Jeans' equation assuming power-law PPSD models. Three different values of α and of χ are shown, matched to highlight the similarity in the density profiles over a large radial range. *Right:* Radial PPSD profiles of Einasto halos compared with power-law models. As in the left panel, the values of α and χ of the three curves have been chosen so as to highlight the similarity of each pair of curves over a wide radial range. In both panels the thick solid curve in black shows the profile corresponding to the billion-particle Aq-A-1 halo, the highest-resolution CDM halo published to date. At the resolution of this halo, or lower, both Einasto and power-law PPSD models provide equally acceptable descriptions of the spherically-averaged structure of CDM halos.

however, these are only evident in regions well inside 1% of the scale radius r_{-2}, and therefore outside the converged region of the highest-resolution simulation of a CDM halo published to date, the Aq-A-1 halo (shown by a solid black line). Deciding whether power-law PPSD models match CDM halos better than Einasto profiles, or vice versa, seems to require simulations of even better resolution than Aq-A-1.

3.6 Power-law PPSD vs Einasto density profile fits

The results above suggest that both Einasto profiles and power-law Q_r models provide equally good representations of the spherically averaged structure of simulated CDM halos, in spite of making very different predictions for their *asymptotic* inner structure.

This conclusion may be verified quantitatively by fitting the "critical" solutions introduced in Sec. 3.4 to the density profiles of all halos in our sample and comparing them with Einasto fits. Residuals from the best fits obtained after varying χ are shown in the bottom panels of Figure 1, and are quite clearly indistinguishable from those obtained by fitting Einasto laws with adjustable α (shown in the middle panels of the same figure).

Further quantitative evidence is provided in Fig. 6, where we plot the figure of merit, ψ_{min}, of the best Einasto fits compared with that obtained from the best-fitting critical solution. Open and filled symbols in this figure are used to denote cases where, respectively, either isotropic or

anisotropic (i.e., β given by eq. (5)) critical solutions have been used in the fitting procedure. The close resemblance of the results obtained with either assumption implies that our conclusions are largely insensitive to our assumption about the radial dependence of the velocity anisotropy.

Finally, our results imply a strong correlation between the best-fitting Einasto's α and "critical" χ parameters for any given halo. We show this in Fig. 7, which suggests that the two parameters are essentially equivalent, and linked by a simple linear relation, $\chi = 2.1 - 1.16\,\alpha$. At the resolution of current simulations, it does not seem possible to decide whether Einasto or power-law PPSDs provide a better description of the spherically-averaged structure of simulated CDM halos.

4 SUMMARY AND CONCLUSIONS

We use a sample of well-resolved equilibrium systems selected from the MS-II simulation in order to study the density and pseudo-phase-space density (PPSD) profiles of CDM halos. In particular, we explore the relation between Einasto profiles (often used to parameterize $\rho(r)$) and power-law PPSD profiles, which are often used to construct equilibrium models of CDM halos.

We solve Jeans' equations to show that the PPSD profiles of Einasto halos are close to power-laws, and that, conversely, the density profiles of power-law PPSD models can be fitted by Einasto laws over a wide radial range. The two
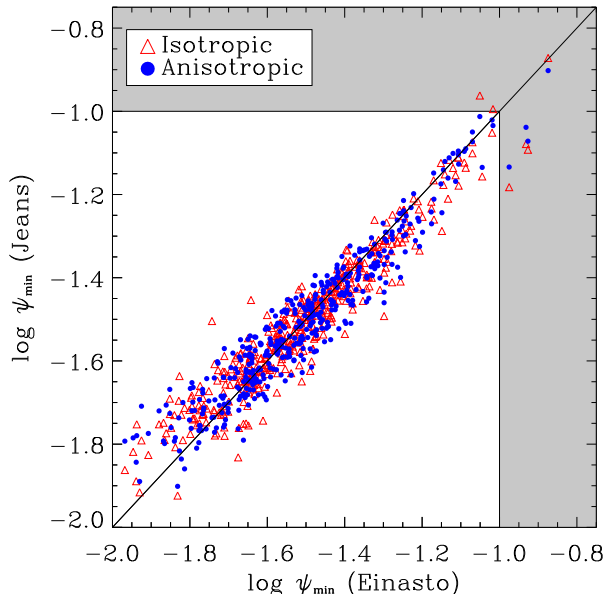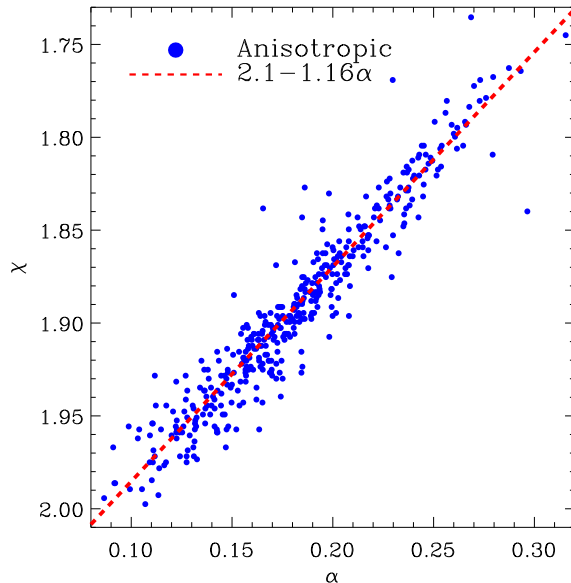
Figure 6. Figure of merit, $\psi_{\min}$, of the best density profile fits to halos in our sample. Values on the y-axis are determined from the best-fitting "critical" power-law Q_r model; those in the abscissa correspond to the best-fitting Einasto profiles. In all cases, fits are limited to the radial range $r_{\rm conv} < r < 3\,r_{-2}$ and have the same number of degrees of freedom: two scale parameters, ρ_{-2} and r_{-2}, and one shape parameter, χ or α. Halos in the shaded grey area have been omitted from the analysis.

Figure 7. The relation between best-fit shape parameters, χ and α, derived from fits to the spherically averaged density profiles using either Einasto profiles or "critical" profiles corresponding to power-law PPSD models. All fits are carried out over the radial range $r_{\rm conv} < r < 3\,r_{-2}$, and assume the anisotropy profile given by eq. (5), with $\beta_\infty = 0.36$ and $A = 0.62$. A dotted line shows the best-fit linear relations, $\chi = 2.1 - 1.16\,\alpha$.

Table 1. Parameters describing the velocity anisotropy profiles (eq. (5))

$\langle \alpha \rangle$	β_∞	A
0.132	0.253	0.720
0.178	0.313	0.656
0.230	0.361	0.618

descriptions differ, however, in their inner asymptotic behaviour, although significant differences are only expected at radii well inside 1% of the scale radius, r_{-2}, and are therefore beyond the reach of current simulations.

Our analysis of the MS-II halo sample shows that, over the resolved radial range, Einasto and power-law PPSD models provide an equally good description of the spherically-averaged structure of simulated CDM halos, provided that the Einasto parameter α and the power-law exponent χ are allowed to float freely when fitting their radial structure. The strong correlation between best-fit α and χ parameters implies that they constitute, in practice, equivalent measures of the shape of the mass profile. These results confirm earlier suggestions that halo structure is not strictly self-similar, and that a "shape" parameter that varies from halo to halo is needed to characterize fully the structure of CDM halos.

The spherically-averaged mass profiles of equilibrium CDM halos thus seem to be fully specified by three parameters: two physical scalings, r_{-2} and ρ_{-2}, and a shape parameter, α or χ. Where CDM halos lie in this three-dimensional parameter space is likely linked to each system's evolutionary history. Exploring the details of these relations remains a pending issue, but one that can be profitably addressed through large-scale numerical efforts such as the Millennium Simulation series. We expect to report progress in this area in the near future.

REFERENCES

Avila-Reese V., Firmani C., Klypin A., Kravtsov A. V., 1999, MNRAS, 310, 527

Bertschinger E., 1985, ApJS, 58, 39

Boylan-Kolchin M., Springel V., White S. D. M., Jenkins A., Lemson G., 2009, MNRAS, 398, 1150

Bullock J. S., Kolatt T. S., Sigad Y., Somerville R. S., Kravtsov A. V., Klypin A. A., Primack J. R., Dekel A., 2001, MNRAS, 321, 559

Dehnen W., McLaughlin D. E., 2005, MNRAS, 363, 1057

Einasto J., 1965, Trudy Inst. Astroz. Alma-Ata, 51, 87

Eke V. R., Navarro J. F., Steinmetz M., 2001, ApJ, 554, 114

Faltenbacher A., Hoffman Y., Gottlöber S., Yepes G., 2007, MNRAS, 376, 1327

Gao L., Navarro J. F., Cole S., Frenk C. S., White S. D. M., Springel V., Jenkins A., Neto A. F., 2008, MNRAS, 387, 536

Hansen S. H., Moore B., 2006, New Astronomy, 11, 333

Hayashi E., White S. D. M., 2008, MNRAS, 388, 2

Jing Y. P., 2000, ApJ, 535, 30

Klypin A., Kravtsov A. V., Bullock J. S., Primack J. R., 2001, ApJ, 554, 903

Kravtsov A. V., Klypin A. A., Khokhlov A. M., 1997, ApJS, 111, 73

Ludlow A. D., Navarro J. F., Springel V., Vogelsberger M., Wang J., White S. D. M., Jenkins A., Frenk C. S., 2010, MNRAS, 406, 137

Ma C., Chang P., Zhang J., 2009, ArXiv e-prints

Merritt D., Graham A. W., Moore B., Diemand J., Terzić B., 2006, AJ, 132, 2685

Merritt D., Navarro J. F., Ludlow A., Jenkins A., 2005, ApJL, 624, L85

Navarro J. F., Frenk C. S., White S. D. M., 1996, ApJ, 462, 563

Navarro J. F., Frenk C. S., White S. D. M., 1997, ApJ, 490, 493

Navarro J. F., Hayashi E., Power C., Jenkins A. R., Frenk C. S., White S. D. M., Springel V., Stadel J., Quinn T. R., 2004, MNRAS, 349, 1039

Navarro J. F., Ludlow A., Springel V., Wang J., Vogelsberger M., White S. D. M., Jenkins A., Frenk C. S., Helmi A., 2010, MNRAS, 402, 21

Neto A. F., Gao L., Bett P., Cole S., Navarro J. F., Frenk C. S., White S. D. M., Springel V., Jenkins A., 2007, MNRAS, 381, 1450

Power C., Navarro J. F., Jenkins A., Frenk C. S., White S. D. M., Springel V., Stadel J., Quinn T., 2003, MNRAS, 338, 14

Rasia E., Tormen G., Moscardini L., 2004, MNRAS, 351, 237

Springel V., White S. D. M., Jenkins A., Frenk C. S., Yoshida N., Gao L., Navarro J., Thacker R., Croton D., Helly J., Peacock J. A., Cole S., Thomas P., Couchman H., Evrard A., Colberg J., Pearce F., 2005, Nature, 435, 629

Taylor J. E., Navarro J. F., 2001, ApJ, 563, 483

Vass I. M., Valluri M., Kravtsov A. V., Kazantzidis S., 2009, MNRAS, 395, 1225